

# The Anomalous Transport of Tracers in Active Baths

Omer Granek,<sup>1</sup> Yariv Kafri,<sup>1</sup> and Julien Tailleur<sup>2</sup>

<sup>1</sup>*Department of Physics, Technion-Israel Institute of Technology, Haifa, 3200003, Israel.*

<sup>2</sup>*Université de Paris, Laboratoire Matière et Systèmes Complexes (MSC), UMR 7057 CNRS, F-75205 Paris, France.*

We derive the long-time dynamics of a tracer immersed in a one-dimensional active bath. In contrast to previous studies, we find that the damping and noise correlations possess long-time tails with exponents that depend on the tracer symmetry. For an asymmetric tracer, the tails lead to superdiffusion and friction that grows with time when the tracer is dragged at a constant speed. For a symmetric tracer, we recover normal diffusion and finite friction. Furthermore, for small symmetric tracers, the noise becomes anticorrelated at late times and the active contribution to the friction becomes negative: active particles then enhance motion rather than oppose it. These results show that, in low-dimensional systems, the motion of a passive tracer in an active bath cannot be modelled as a persistent random walker with a finite correlation time.

Since Einstein, Smoluchowski and Langevin, the Brownian motion of tracer particles in a bath has been a topic of much interest [1]. When compared to the equilibrium case, the problem of an active bath reveals a much richer physics, from the ratchet motion induced by asymmetric gears [2–5] and rectifiers [6–11] to the long-ranged forces and currents generated by asymmetric obstacles [11–15]. In spite of two decades of experimental, theoretical, and numerical studies [16–47], a comprehensive theory for the motion of passive tracers in active baths is still lacking.

To fill this gap, one would like to derive a generalized Langevin equation (GLE) for the tracer dynamics. In 1D, this takes the form

$$\gamma_0 \dot{X}(t) + \int_0^t dt' \gamma(t-t') \dot{X}(t') = \mathcal{F}(t) + \eta(t), \quad (1)$$

where the interactions with the active particles lead to a stochastic force  $\mathcal{F}(t)$  and a retarded friction  $\int_0^t dt' \gamma(t-t') \dot{X}(t')$ . In addition, Eq. (1) includes a memoryless viscous medium at temperature  $T$  that leads to the friction coefficient  $\gamma_0$  and a Gaussian white noise  $\eta(t)$  satisfying  $\langle \eta(t)\eta(t') \rangle = 2\gamma_0 T \delta(t-t')$  [48]. Note that the tracers dynamics can be described by Eq. (1) only in the adiabatic limit in which  $\gamma_0$  is large so that the bath's relaxation is much faster than the tracer's response [49–56]. So far, experimental and numerical studies [16–26] have suggested that the random, finite-duration encounters between the bath particles and the tracer lead to a friction  $\gamma(t)$  that decays exponentially over a short timescale, so that the tracer dynamics reduces to  $(\gamma_0 + \gamma_T) \dot{X}(t) = \mathcal{F}(t)$ , where  $\gamma_T \equiv \int_0^\infty dt \gamma(t)$ . In addition, the large-scale motion of the tracer is always found to be diffusive.

Despite much recent work at the analytical level, to the best of our knowledge, no systematic derivation to date provides explicit, closed expressions for  $\gamma(t-t')$  and  $\mathcal{F}(t)$  starting from microscopic models of generic active baths and tracers. Indeed, such derivations are notoriously difficult and often require approximations or simplifications, even in equilibrium where exact results are scarce [57–59]. For instance, recent works on active baths have treated the encounters between bath particles and tracers as independent Poisson pro-

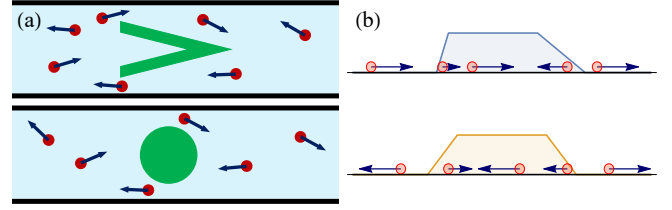


Figure 1. (a) A large tracer and a bath of small active particles are immersed in a viscous medium inside a long narrow channel. (b) The short transverse dimension allows modelling the channel as a one-dimensional system where particles can bypass each other and the tracer, even though the transverse and orientational fluctuations of the tracer are lost in this one-dimensional description. Top: asymmetric tracer. Bottom: symmetric tracer.

cesses [45], have modelled their interactions using a weak confining harmonic potential [60], or have relied on mode-coupling approximations [61, 62]. Invariably, all these works lead to a diffusive long-time behavior, in agreement with pre-existing results [63–66].

All the approaches above suffer from a major issue: The short-time memory and correlation picture is necessarily incomplete because the fluctuating density of active particles is a conserved quantity. As such, the bath does not have a single characteristic relaxation time due to the existence of a slow hydrodynamic field. This should, generically, lead to power-law memory and correlations [67–72]. In low-dimensional systems, these tails may result in anomalous transport over long timescales when the friction coefficient  $\gamma_T$  or noise intensity  $I \equiv \int_0^\infty dt C_{\mathcal{F}}(t)$  diverge. Although thoroughly studied in equilibrium systems, where these effects were shown to lead to a host of unexpected behaviours such as the breakdown of the Fourier law and local hydrodynamics [73–75], these effects were so far widely overlooked in active matter.

In this Letter, to resolve this issue, we consider the simplest non-trivial system in which Eq. (1) can be systematically derived. We thus study a single tracer immersed in a dry one-dimensional active bath of run-and-tumble particles. To remain as close as possible to the phenomenology of an active bath in  $d > 1$  dimensions, we allow particles to overtake each other and the tracer, hence modelling the latter by a

soft repulsive potential  $V(x)$ , see Fig. 1. Starting from the coupled dynamics of the bath particle and tracer positions,  $\{x_i(t), X(t)\}$ , we determine explicitly the long-time behaviors of  $\gamma(t)$  and  $C_{\mathcal{F}}(t)$  as functions of the tracer shape and of the microscopic parameters of our model. To do so, we employ a *controlled* adiabatic expansion [76, 77] valid in the large  $\gamma_0$  limit in which the tracer dynamics can be described by Eq. (1). Our results show that the return statistics of the active particles exhibit long-time tails that were previously overlooked. These lead to interesting and qualitatively different behaviors for symmetric and asymmetric tracers. For *asymmetric* tracers,  $\gamma(t)$  and  $C_{\mathcal{F}}(t)$  scale as  $\sim t^{-1/2}$  in the long-time limit, leading to *superdiffusive* behavior around their mean displacements:

$$\langle X^2(t) \rangle_c \equiv \langle X^2(t) \rangle - \langle X(t) \rangle^2 \sim Kt^{3/2}. \quad (2)$$

When the tracer is towed at a constant velocity  $U$ , it experiences a friction force from the active particles that grows as:

$$\frac{f_{\text{fric}}(t)}{U} \sim -\Gamma_{\text{T}} t^{1/2}. \quad (3)$$

We provide below explicit expressions for  $K$  and  $\Gamma_{\text{T}}$  in the presence of a soft asymmetric potential in a dilute active bath. For a *symmetric* tracer,  $C_{\mathcal{F}}(t)$  and  $\gamma(t)$  scale as  $\sim t^{-3/2}$ , similar to a tracer in a bath of equilibrium Brownian particles [68, 78], which yields a *diffusive* behavior:

$$\langle X^2(t) \rangle_c \sim 2Dt. \quad (4)$$

Towing the tracer at constant velocity  $U$ , the active particles exert a *finite* friction force:

$$\frac{f_{\text{fric}}(t)}{U} = -\gamma_{\text{T}} - \gamma_1 t^{-1/2} + \mathcal{O}(t^{-3/2}), \quad (5)$$

where  $\gamma_{\text{T}} \equiv \int_0^\infty dt \gamma(t)$ . Interestingly, for small tracer sizes,  $\gamma_{\text{T}}$  and  $\gamma_1$  are negative: the active bath pushes the tracer in the towing direction. We provide perturbative expressions for  $D$  and  $\gamma_{\text{T}}$  and defer their systematic derivations for later work [79]. All our results are confirmed by microscopic simulations shown in Fig. 2. The derivation presented below suggests that the exponents are *universal* to any bath with long-time diffusive statistics. We confirm that they hold in the presence of soft repulsive interparticle forces in Section I of the SM [80].

*Model.* We consider bath particles moving with speed  $v$  and randomly switching their orientations with rate  $\alpha/2$ , leading to a persistence length  $\ell_p = v/\alpha$ . The tracer interacts with the active bath via a short-range potential  $V$  which vanishes outside  $[0, L_{\text{T}}]$ , such that the force on bath particle  $i$  is  $f(x_i - X) = -\partial_{x_i} V(x_i - X)$  and the tracer size is  $L_{\text{T}}$ . We take  $|\mu f(x)| < v$  so that particles are able to cross the tracer, which emulates the channel in Fig. 1a. The tracer and bath-particle

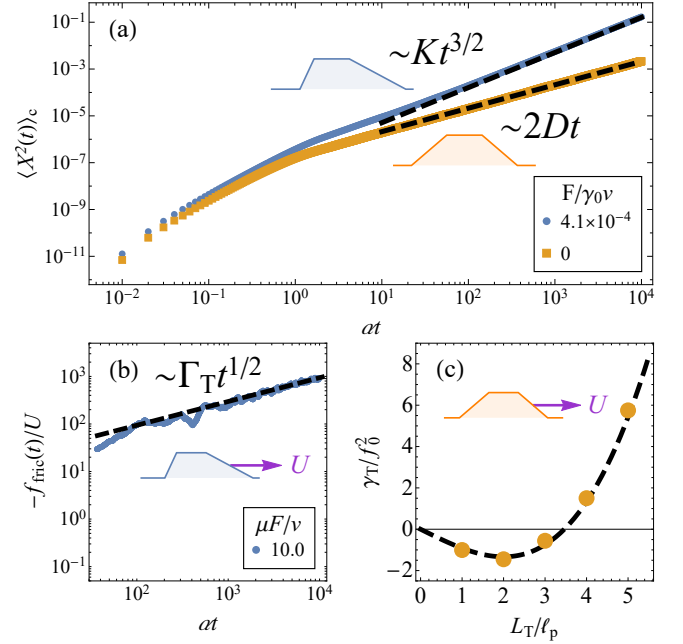


Figure 2. Simulation results (symbols) compared with our theoretical predictions for the long-time limit, without any fitting parameters, (dashed black lines): (a) MSD for symmetric and asymmetric tracers; (b) friction force exerted on an asymmetric tracer; (c) symmetric-tracer friction coefficient vs tracer size  $L_{\text{T}}$ . Simulation details and results for soft repulsive interactions are given in Section I of [80].

dynamics thus read

$$\gamma_0 \dot{X}(t) = F_{\text{tot}}(t) \equiv - \sum_i f[x_i(t) - X(t)], \quad (6)$$

$$\dot{x}_i(t) = v\sigma_i(t) + \mu f[x_i(t) - X(t)], \quad (7)$$

where the  $\sigma_i(t) \in \{\pm 1\}$  flip independently with rate  $\alpha/2$  and  $\mu$  is the bath-particle mobility. In Eqs. (6) and (7) we neglected the thermal noises acting on the tracer and bath particles, which are typically much weaker than the active and viscous forces [16, 17, 25, 29, 81]. In the analytical derivations below we consider a dilute bath of active particles, without interparticle forces, in either infinite systems or periodic ones of size  $L \gg L_{\text{T}}, \ell_p$ .

*Theory.* The fluctuating force  $F_{\text{tot}}(t)$  differs from the average force  $F$  exerted on a tracer held *fixed*. This is due to both the tracer's motion and the stochasticity of the active bath. The average correction due to the tracer motion is characterised by  $\gamma(t)$  in Eq. (1). Within an adiabatic perturbation theory  $\gamma(t)$  is defined as

$$\langle F_{\text{tot}}(t) \rangle - F \equiv - \int_0^t dt' \gamma(t-t') \dot{X}(t'), \quad (8)$$

where the average is conditioned on a given realization of

$\dot{X}(t)$ . The fluctuations of  $F_{\text{tot}}$  are then characterized through

$$\mathcal{F}(t) \equiv F_{\text{tot}}(t) + \int_0^t dt' \gamma(t-t') \dot{X}(t'). \quad (9)$$

Adiabatic perturbation theory tells us that, when  $\gamma_0$  is large, the statistics of  $\mathcal{F}(t)$  are identical to those of the force exerted on a tracer held fixed [77]. Furthermore, it relates  $\gamma(t)$  and  $\mathcal{F}(t)$  through an Agarwal-Kubo-type formula [76]

$$\gamma(t-t') = \langle \mathcal{F}(t) \partial_{X_0} \ln \rho_s [x(t') - X_0, \sigma(t')] \rangle^s. \quad (10)$$

Here,  $\rho_s(x - X_0, \sigma)$  is the steady-state density of bath particles with orientation  $\sigma$  and displacement  $x - X_0$  from a tracer held fixed at  $X_0$ . The brackets  $\langle \cdot \rangle^s$  represent an average with respect to  $\rho_s$ . In the following, we set  $X_0 = 0$  without loss of generality. For an equilibrium bath at temperature  $T$ ,  $\langle \mathcal{F}(t) \rangle^s = 0$  and Eq. (10) reduces to the fluctuation-dissipation theorem  $\gamma(t) = C_{\mathcal{F}}(t)/T$  where  $C_{\mathcal{F}}(t) = \langle \mathcal{F}(t) \mathcal{F}(0) \rangle^s$ . Outside equilibrium, these constraints need not hold.

To characterize the tracer dynamics, we compute independently  $F = \langle \mathcal{F}(t) \rangle^s$ ,  $C_{\mathcal{F}}(t)$  and  $\gamma(t-t')$ . To do so, we start from the expression for the steady state of noninteracting run-and-tumble particles in the presence of an external force  $f(x)$  [82, 83]:

$$\rho_s(x, \sigma) = \frac{\frac{1}{2}\rho_L}{1 + \sigma \frac{\mu}{v} f(x)} \exp \left\{ \beta_{\text{eff}} \int_0^x dy \frac{f(y)}{1 - [\frac{\mu}{v} f(y)]^2} \right\}, \quad (11)$$

where  $\rho_L$  is the particle density at  $x = 0^-$ ,  $T_{\text{eff}} = v^2/\mu\alpha$  is the effective temperature, and  $\beta_{\text{eff}} = 1/T_{\text{eff}}$ . The steady-state density is  $\rho_s(x) = \sum_{\sigma} \rho_s(x, \sigma)$ .

*Asymmetric tracer.* For an asymmetric tracer, the densities of active particles  $\rho_R$  and  $\rho_L$  at the right and left ends of the tracer differ and are given by  $\rho_R = 2\rho_0/[1 + \exp(\beta_{\text{eff}}\varepsilon)]$  and  $\rho_L = 2\rho_0/[1 + \exp(-\beta_{\text{eff}}\varepsilon)]$ , where  $\varepsilon \equiv -\int dx f(x)/\{1 - [\mu f(x)/v]^2\}$ . The density difference then leads to a nonvanishing average force  $F = -\int dx x f(x) \rho_s(x)$  exerted on the tracer [12, 84, 85], which is given by

$$F = -T_{\text{eff}}(\rho_R - \rho_L) = 2T_{\text{eff}}\rho_0 \tanh \left( \frac{\varepsilon}{2T_{\text{eff}}} \right), \quad (12)$$

where we have introduced the average background density  $\rho_0 = (\rho_R + \rho_L)/2$ . Note that Eq. (12) is consistent with the ideal gas law applied to the left and right sides of the tracer.

The long-time behavior of  $C_{\mathcal{F}}(t)$  and  $\gamma(t)$  can be derived from the knowledge of the propagator  $p(x, \sigma, t|x', \sigma', 0)$ . In the long-time limit, the dynamics of the active particles are diffusive so that the support of  $p(x, \sigma, t|x', \sigma', 0)$  spreads over a region of length  $2b(t)$  around  $x'$ , where  $b(t) \sim (\pi D_{\text{eff}} t)^{1/2}$  is a diffusive propagating front. For any  $x - x' \ll b(t)$ , and to leading order in  $b(t)$ ,  $p(x, \sigma, t|x', \sigma', 0)$  has relaxed to the normalized steady-state distribution  $\rho_s(x, \sigma)/\sum_{\sigma} \int_{-b(t)}^{b(t)} dx \rho_s(x, \sigma)$ . For  $L_T \ll 2b(t)$ ,

one can neglect the region inside the tracer in the integral so that  $\sum_{\sigma} \int_{-b(t)}^{b(t)} dx \rho_s(x, \sigma) \sim (\rho_R + \rho_L)b(t)$ , up to corrections of order  $\mathcal{O}(L^{-1})$ . Since  $b(t) \sim (\pi D_{\text{eff}} t)^{1/2}$  we get

$$p(x, \sigma, t|x', \sigma', 0) \sim \frac{\rho_s(x, \sigma)}{\rho_R + \rho_L} (\pi D_{\text{eff}} t)^{-1/2}. \quad (13)$$

This heuristic result can be derived exactly, within the adiabatic limit, and its sub-leading correction can be shown to scale as  $\mathcal{O}(t^{-3/2})$  (See Section II of [80]).

On long times,  $p(x, \sigma, t|x', \sigma', 0)$  is independent of the initial coordinate  $(x', \sigma')$ . Therefore, two-point correlations are factorized in this limit. Furthermore, for  $N$  noninteracting particles, the forces exerted by different particles on the tracer are uncorrelated so that  $C_{\mathcal{F}}(t) = N\{\langle f(t)f(0) \rangle^s - [\langle f(t) \rangle^s]^2\}$ , where  $f(t)$  is the force due to a single bath particle. Since  $\langle f(t) \rangle^s = F/N$ ,  $N[\langle f(t) \rangle^s]^2$  only contributes a correction of order  $\mathcal{O}(L^{-1})$  to  $C_{\mathcal{F}}(t)$ . Using Eq. (II.38),  $C_{\mathcal{F}}(t)$  can then be evaluated as:

$$C_{\mathcal{F}}(t) = \sum_{\sigma\sigma'} \int dx dx' f(x) p(x, \sigma, t|x', \sigma', 0) f(x') \rho_s(x', \sigma') \quad (14)$$

$$= \frac{F^2}{\rho_R + \rho_L} (\pi D_{\text{eff}} t)^{-1/2} + \mathcal{O}(t^{-3/2}). \quad (15)$$

Similarly, we obtain from Eqs. (10) and (12)

$$\gamma(t) = \sum_{\sigma\sigma'} \int dx dx' f(x) p(x, \sigma, t|x', \sigma', 0) \partial_{x'} \rho_s(x', \sigma') \quad (16)$$

$$= \beta_{\text{eff}} \frac{F^2}{\rho_R + \rho_L} (\pi D_{\text{eff}} t)^{-1/2} + \mathcal{O}(t^{-3/2}). \quad (17)$$

We note that Eqs (11)-(17) hold in the infinite-system-size limit. For large-but-finite systems, they are complemented by  $\mathcal{O}(L^{-1})$  corrections, as discussed in Section III of [80].

Equations (15) and (17) immediately show that the asymmetric tracer undergoes anomalous dynamics on long times. Indeed, the noise and friction intensities, defined as  $I = \int_0^\infty dt C_{\mathcal{F}}(t)$  and  $\gamma_T = \int_0^\infty dt \gamma(t)$  are infinite, hence leading to an ill-defined diffusivity  $D \equiv I/(\gamma_0 + \gamma_T)^2$ . To characterize the anomalous dynamics of the tracer we first consider its free motion. We define the tracer's mobility  $B(t)$  through  $X(t) = \int_0^t dt' B(t-t') \mathcal{F}(t')$ , which leads to

$$\langle X(t)^2 \rangle_c = 2 \int_0^t dt_1 \int_0^{t_1} dt_2 B(t_1) B(t_2) C_{\mathcal{F}}(t_1 - t_2). \quad (18)$$

Since we are working in the large  $\gamma_0$  limit,  $B(t) \sim 1/\gamma_0$  [86]. Using Eq. (15) for  $C_{\mathcal{F}}(t)$  then gives Eq. (2), hence implying *superdiffusion*, with

$$K = \frac{4F^2}{3\rho_0\gamma_0^2\sqrt{\pi D_{\text{eff}}}}. \quad (19)$$

In addition to anomalous diffusion, the asymmetric tracer experiences friction that grows with time, as shown by the

following towing experiment. Setting a constant velocity  $\dot{X} = U$  in Eq. (1), the friction exerted by the active particles on the tracer can be measured as  $f_{\text{fric}}(t) \equiv \langle F_{\text{tot}} \rangle - F$ . From Eqs. (8) and (17), we get

$$f_{\text{fric}}(t) = -U \int_0^t dt' \gamma(t') \sim -U \frac{F^2}{T_{\text{eff}} \rho_0} \left( \frac{t}{\pi D_{\text{eff}}} \right)^{1/2}, \quad (20)$$

which yields Eq. (5) with  $\Gamma_{\text{T}} = F^2 (\pi D_{\text{eff}})^{-1/2} / T_{\text{eff}} \rho_0$ .

*Symmetric tracer.* For a symmetric tracer,  $F = 0$ . Equations (15) and (17) then imply that  $\gamma(t)$ ,  $C_{\mathcal{F}}(t) = \mathcal{O}(t^{-3/2})$ . In this case,  $I$  and  $\gamma_{\text{T}}$  remain finite so that  $D = I / (\gamma_0 + \gamma_{\text{T}})^2$  is well defined and Eq. (4) holds. We now present heuristic discussions of  $C_{\mathcal{F}}(t)$  and  $\gamma(t)$  that account for two important features: their scaling as  $t^{-3/2}$  and their sign changes for small tracers. These results can be derived exactly, within the adiabatic limit, for piecewise linear potentials [79].

Consider a symmetric tracer of length  $L_{\text{T}}$  whose potential is depicted in Fig. 3. While our results can be derived exactly [79], we present here a simple argument which holds in the limit in which the edges of the tracer have a small width  $d$  and small slopes  $\pm f_0$ . Consider first a single particle located at the left end of the tracer, at  $\hat{x} \simeq 0$ , moving in the direction  $\hat{\sigma}$ . At long times, the probability distribution of its position  $x$  is a Gaussian centered around  $\hat{\sigma} \ell_p$ , of variance  $2D_{\text{eff}} t$  (See Fig. 3). The force-force correlation of this particle can be computed as

$$c(\hat{\sigma}, t) = \frac{f_0^2 d}{\sqrt{4\pi D_{\text{eff}} t}} \left[ e^{-\frac{\ell_p^2}{4D_{\text{eff}} t}} - e^{-\frac{(L_{\text{T}} - \hat{\sigma} \ell_p)^2}{4D_{\text{eff}} t}} \right], \quad (21)$$

as can be inferred from Eq. (14) using  $\rho_s(x', \sigma') = \delta(x') \delta_{\sigma', \hat{\sigma}}$ . Note that the factor  $d$  comes from the integration over  $x$  in Eq. (14), which also leads to the two exponentials corresponding to  $x \simeq 0$  and  $x \simeq L_{\text{T}}$ , respectively. This amounts to summing the contribution due to particles returning to the left end, such that  $f(x)f(x') = f_0^2$ , and that of particles crossing the tracer, such that  $f(x)f(x') = -f_0^2$ .

Let us return to the case of an active bath of density  $\rho_0$ . We denote by  $m$  the polarization of particles around  $x' = 0$  so that the local density of particles with orientation  $\sigma$  is  $\rho_0 \frac{1+\sigma m}{2}$ . The force-force correlation is then obtained from the single-particle result through  $C_{\mathcal{F}}(t) = 2\rho_0 [\frac{1+m}{2} c(1, t) + \frac{1-m}{2} c(-1, t)]$ , where the factor 2 stems from the contributions of particles starting at  $x' \simeq L_{\text{T}}$ . Expanding the exponentials in (21) in the long-time limit, one finds the leading orders to cancel, yielding the  $t^{-3/2}$  scaling of  $C_{\mathcal{F}}(t)$ . Using Eq. (11) leads to  $m = \mu f_0 / v$ , which is consistent with the fact that active particles polarize against external potentials [87]. Straightforward algebra then gives

$$C_{\mathcal{F}}(t) \sim \frac{\rho_0 (f_0 d L_{\text{T}})^2}{4\pi^{1/2} (D_{\text{eff}} t)^{3/2}} G(\ell_p / L_{\text{T}}) \quad (22)$$

where  $G(y) = 1 - \frac{2\mu f_0}{v} y$ . Importantly,  $C_{\mathcal{F}}(t)$  becomes negative when the size of the tracer is small,  $L_{\text{T}} \leq 2\mu \ell_p f_0 / v$ . In the discussion above, we neglected  $\mathcal{O}(f_0)$  corrections to

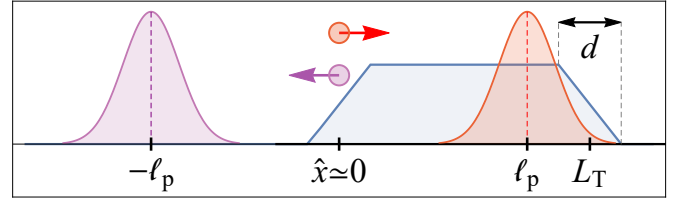


Figure 3. Consider a symmetric tracer (blue potential) and an active particle located at its left end at position  $\hat{x}$  at  $t = 0$ . The particle is shown in orange and magenta for  $\hat{\sigma} = \pm 1$  respectively. At late times, the particle position is distributed as a Gaussian centered around  $x_c = \hat{x} + \hat{\sigma} \ell_p$ . For  $\hat{\sigma} = 1$ , when  $\ell_p \gg L_{\text{T}}$ , the anticorrelation between  $f(x')$  and  $f(x)$  leads to a negative contribution to  $C_{\mathcal{F}}(t)$ . Conversely, a  $\hat{\sigma} = -1$  particle leads to a positive contribution to  $C_{\mathcal{F}}(t)$ . Due to the polarization against the potential,  $\hat{\sigma} = \pm 1$  occur with different probabilities. This leads to an overall negative  $C_{\mathcal{F}}(t)$  for small  $L_{\text{T}}$  and a positive one for large sizes.

the propagator and to the steady-state density due to the edges of the tracer. Including the  $f_0$  corrections to all orders confirms the scaling (22), to order  $\mathcal{O}(d^2)$ , albeit with  $G(y) = [1 - (\frac{2\mu f_0 y}{v})^2] / [1 - (\frac{\mu f_0}{v})^2]^2$  (See Section IV of [80]). This does not change the leading order estimate for the crossover length  $\sim 2\mu f_0 \ell_p / v$ . Finally, we stress that the change of sign of  $C_{\mathcal{F}}(t)$  is a direct consequence of the polarization against the potential. Setting  $m = 0$  in the computation above always leads to  $C_{\mathcal{F}}(t) > 0$ .

We now turn to the long-time behavior of  $\gamma(t)$ . Inserting Eq. (11) in Eq. (10) leads to  $\gamma = \gamma_p - \gamma_a$ , with

$$\gamma_p(t - t') \equiv \beta_{\text{eff}} \left\langle \mathcal{F}(t) \frac{\mathcal{F}(t')}{1 - [\frac{\mu}{v} \mathcal{F}(t')]^2} \right\rangle_c, \quad (23)$$

$$\gamma_a(t - t') \equiv \beta_{\text{eff}} \left\langle \mathcal{F}(t) \frac{\sigma(t') \ell_p \partial_{x(t')} \mathcal{F}(t')}{1 - \sigma(t') \frac{\mu}{v} \mathcal{F}(t')} \right\rangle_c. \quad (24)$$

The heuristic argument developed above for  $C_{\mathcal{F}}(t)$  directly extends to the correlators (23) and (24), showing that  $\gamma_a$  and  $\gamma_p$  both inherit the  $t^{-3/2}$  scaling of  $C_{\mathcal{F}}(t)$  at long times. Inspecting Eq. (23) shows that, to leading order in  $f_0$ ,

$$\gamma_p(t) \sim \beta_{\text{eff}} C_{\mathcal{F}}(t) = \frac{\beta_{\text{eff}} \rho_0 (f_0 d L_{\text{T}})^2}{4\pi^{1/2} (D_{\text{eff}} t)^{3/2}} G(\ell_p / L_{\text{T}}). \quad (25)$$

The presence of  $\sigma(t')$  in Eq. (24) makes the contributions of  $\sigma' = \pm 1$  particle add up, instead of cancelling, leading to  $\gamma_a(t) > 0$  for all  $L_{\text{T}}$  and a long-time scaling  $\gamma_a \sim \mathcal{O}(f_0^3) t^{-3/2}$ . Therefore, to leading order in  $f_0$ ,  $\gamma \sim \beta_{\text{eff}} C_{\mathcal{F}}(t)$ . This suggests that  $\gamma_{\text{T}} = \int_0^\infty dt \gamma(t)$  can also change sign and become *negative* for small tracers. Indeed, a perturbative calculation finds that

$$\gamma_{\text{T}} \sim \beta_{\text{eff}} v^{-1} \rho_0 (f_0 d)^2 \frac{L_{\text{T}}}{\ell_p} \left( 1 - \frac{d^2 + 6\ell_p^2}{3dL_{\text{T}}} \right). \quad (26)$$

The derivations of this result and of the asymptotics of  $\gamma_a$  are

not particularly illuminating; they are deferred to Section IV of [80]. Importantly, Eq. (IV.14) implies that when a small symmetric tracer is dragged at velocity  $U$ , the active bath *enhances* its motion rather than resisting it.

*Adiabatic limit.* Although Eq. (1) is a common framework to describe tracer's dynamics, it relies on the assumption that their motion is slow. An important—but rarely debated—question is thus its range of validity. Here, this is set by the requirement that the tracer's response is much slower than the diffusive relaxation of the bath, *i.e.*  $\langle X(t) \rangle, \langle X^2(t) \rangle_c^{1/2} \ll (D_{\text{eff}}t)^{1/2}$ . For an asymmetric tracer, using  $\langle X(t) \rangle \sim Ft/\gamma_0$  and Eq. (2), we find  $t \ll \tau_1 \equiv D_{\text{eff}}(\gamma_0/F)^2$  and  $t \ll \tau_2 \equiv (D_{\text{eff}}/K)^2$ . Equation (19) implies  $\tau_1 \ll \tau_2$  so that the adiabatic limit holds up to  $t \ll \tau_1$ . Beyond this time scale, which can be arbitrarily large, an asymmetric tracer in an active bath cannot be described by Eq. (1). Considering a finite system of size  $L$ , the diffusive relaxation time is  $t = \tau_{\text{rel}} \sim L^2/D_{\text{eff}}$ . Thus, the adiabatic limit for an asymmetric tracer in a finite system is valid for  $FL \ll D_{\text{eff}}\gamma_0$ , which can be achieved by designing the tracer shape to bound  $F$  or by using a small enough system. For a symmetric tracer, there is no temporal restriction and the only requirement is  $D \ll D_{\text{eff}}$ , which can be fulfilled by setting  $\gamma_0 \gg (I/D_{\text{eff}})^{1/2}$ . For towing both asymmetric tracers and symmetric tracers at constant velocity  $U$ , the only requirement is  $U \ll D_{\text{eff}}/L$ .

*Conclusion.* In this Letter, we have derived the long-time dynamics of a passive tracer in a dilute active bath under the sole assumption of an adiabatic evolution. We have revealed new regimes for both asymmetric and symmetric tracers. First, long-time tails lead to the superdiffusion of asymmetric tracers, which also experience friction that grows with time when they are dragged at constant velocity  $U$ . For symmetric tracers, the long-time tail preserves the diffusive behavior, but negative active friction is observed for small tracers. The latter solely follows from the persistent motion of active particles and their polarization by external potentials, a mechanism that differs from previously studied cases with negative mobility [60, 88, 89]. We expect the tails for asymmetric and symmetric tracers to become  $t^{-d/2}$  and  $t^{-(d/2+1)}$  in  $d$  dimensions, respectively. This suggests, in two dimensions, that  $\langle X(t)^2 \rangle_c \sim t \ln t$  for an asymmetric tracer, which remains to be verified [90]. Our results stemmed from generic and straightforward features of active particles already present in dilute diffusive settings and were shown numerically to extend to interacting active particles. Our result show the exponents to be universal while the transport coefficients are dressed by interactions. Moreover, the mechanisms should lead to even richer behaviours for active suspensions in momentum-conserving fluids [33, 38, 39, 45]. These are likely to yield even slower decaying power laws and anomalous statistics.

*Acknowledgements.* We thank Yongjoo Baek, Bernard Derida, and Xinpeng Xu for many useful discussions. OG and YK are supported by an Israel Science Foundation grant (1331/17) and an NSF-BSF grant (2016624). JT is supported by the ANR grant THEMA.

- [1] P. Hänggi and F. Marchesoni, *Chaos An Interdiscip. J. Nonlinear Sci.* **15**, 026101 (2005).
- [2] R. Di Leonardo, L. Angelani, D. Dell'Arciprete, G. Ruocco, V. Iebba, S. Schippa, M. P. Conte, F. Mecarini, F. De Angelis, and E. Di Fabrizio, *Proc. Natl. Acad. Sci.* **107**, 9541 (2010).
- [3] A. Sokolov, M. M. Apodaca, B. A. Grzybowski, and I. S. Aranson, *Proc. Natl. Acad. Sci.* **107**, 969 (2010).
- [4] A. Kaiser, A. Peshkov, A. Sokolov, B. ten Hagen, H. Löwen, and I. S. Aranson, *Phys. Rev. Lett.* **112**, 158101 (2014).
- [5] C. Maggi, F. Saglimbeni, M. Dipalo, F. De Angelis, and R. Di Leonardo, *Nat. Commun.* **6**, 7855 (2015).
- [6] P. Galajda, J. Keymer, P. Chaikin, and R. Austin, *J. Bacteriol.* **189**, 8704 (2007).
- [7] M. B. Wan, C. J. Olson Reichhardt, Z. Nussinov, and C. Reichhardt, *Phys. Rev. Lett.* **101**, 018102 (2008).
- [8] J. Tailleur and M. E. Cates, *EPL* **86**, 60002 (2009).
- [9] J. Stenhammar, R. Wittkowski, D. Marenduzzo, and M. E. Cates, *Sci. Adv.* **2**, e1501850 (2016).
- [10] C. O. Reichhardt and C. Reichhardt, *Annu. Rev. Condens. Matter Phys.* **8**, 51 (2017).
- [11] T. Speck, *Soft Matter* **16**, 2652 (2020).
- [12] N. Nikola, A. P. Solon, Y. Kafri, M. Kardar, J. Tailleur, and R. Voituriez, *Phys. Rev. Lett.* **117**, 098001 (2016).
- [13] Y. Baek, A. P. Solon, X. Xu, N. Nikola, and Y. Kafri, *Phys. Rev. Lett.* **120**, 058002 (2018).
- [14] O. Granek, Y. Baek, Y. Kafri, and A. P. Solon, *J. Stat. Mech. Theory Exp.* **2020**, 063211 (2020).
- [15] T. Speck and A. Jayaram, *Phys. Rev. Lett.* **126**, 138002 (2021).
- [16] X.-L. Wu and A. Libchaber, *Phys. Rev. Lett.* **84**, 3017 (2000).
- [17] C. Maggi, M. Paoluzzi, N. Pellicciotta, A. Lepore, L. Angelani, and R. Di Leonardo, *Phys. Rev. Lett.* **113**, 238303 (2014).
- [18] A. Argun, A.-R. Moradi, E. Pinçe, G. B. Bağcı, A. Imparato, and G. Volpe, *Phys. Rev. E* **94**, 062150 (2016).
- [19] C. Maggi, M. Paoluzzi, L. Angelani, and R. Di Leonardo, *Sci. Rep.* **7**, 17588 (2017).
- [20] S. Chaki and R. Chakrabarti, *Phys. A Stat. Mech. its Appl.* **511**, 302 (2018).
- [21] S. Chaki and R. Chakrabarti, *Physica A* **530**, 121574 (2019).
- [22] L. Dabelow, S. Bo, and R. Eichhorn, *Phys. Rev. X* **9**, 021009 (2019).
- [23] K. Goswami, *Phys. Rev. E* **99**, 012112 (2019).
- [24] M. Knežević and H. Stark, *New J. Phys.* **22**, 113025 (2020).
- [25] S. Ye, P. Liu, F. Ye, K. Chen, and M. Yang, *Soft Matter* **16**, 4655 (2020).
- [26] S. Belan and M. Kardar, *J. Chem. Phys.* **154**, 024109 (2021).
- [27] G. Soni, B. Jaffar Ali, Y. Hatwalne, and G. Shivashankar, *Biophys. J.* **84**, 2634 (2003).
- [28] D. T. N. Chen, A. W. C. Lau, L. A. Hough, M. F. Islam, M. Goulian, T. C. Lubensky, and A. G. Yodh, *Phys. Rev. Lett.* **99**, 148302 (2007).
- [29] D. Loi, S. Mossa, and L. F. Cugliandolo, *Phys. Rev. E* **77**, 051111 (2008).
- [30] P. T. Underhill, J. P. Hernandez-Ortiz, and M. D. Graham, *Phys. Rev. Lett.* **100**, 248101 (2008).
- [31] A. W. C. Lau and T. C. Lubensky, *Phys. Rev. E* **80**, 011917 (2009).
- [32] K. C. Leptos, J. S. Guasto, J. P. Gollub, A. I. Pesci, and R. E. Goldstein, *Phys. Rev. Lett.* **103**, 198103 (2009).
- [33] J. Dunkel, V. B. Putz, I. M. Zaid, and J. M. Yeomans, *Soft Matter* **6**, 4268 (2010).
- [34] H. Kurtuldu, J. S. Guasto, K. A. Johnson, and J. P. Gollub, *Proc.*

- Natl. Acad. Sci. U.S.A **108**, 10391 (2011).
- [35] G. Miño, T. E. Mallouk, T. Darnige, M. Hoyos, J. Dauchet, J. Dunstan, R. Soto, Y. Wang, A. Rousselet, and E. Clement, *Phys. Rev. Lett.* **106**, 048102 (2011).
- [36] G. Foffano, J. S. Lintuvuori, K. Stratford, M. E. Cates, and D. Marenduzzo, *Phys. Rev. Lett.* **109**, 028103 (2012).
- [37] G. L. Miño, J. Dunstan, A. Rousselet, E. Clément, and R. Soto, *J. Fluid Mech.* **729**, 423 (2013).
- [38] A. Morozov and D. Marenduzzo, *Soft Matter* **10**, 2748 (2014).
- [39] J.-L. Thiffeault, *Phys. Rev. E* **92**, 023023 (2015).
- [40] A. E. Patteson, A. Gopinath, P. K. Purohit, and P. E. Arratia, *Soft Matter* **12**, 2365 (2016).
- [41] A. Suma, L. F. Cugliandolo, and G. Gonnella, *J. Stat. Mech: Theory Exp.* **2016**, 054029 (2016).
- [42] M. J. Y. Jerez, M. N. P. Confesor, M. V. Carpio Bernido, and C. C. Bernido, in *AIP Conference Proceedings*, Vol. 1871 (2017) p. 050004.
- [43] T. Kurihara, M. Aridome, H. Ayade, I. Zaid, and D. Mizuno, *Phys. Rev. E* **95**, 030601(R) (2017).
- [44] R. Chatterjee, N. Segall, C. Merrigan, K. Ramola, B. Chakraborty, and Y. Shokef, *J. Chem. Phys.* **150**, 144508 (2019).
- [45] K. Kanazawa, T. G. Sano, A. Cairoli, and A. Baule, *Nature* **579**, 364 (2020).
- [46] L. Abbaspour and S. Klumpp, *Phys. Rev. E* **103**, 052601 (2021).
- [47] J. Katuri, W. E. Uspal, M. N. Popescu, and S. Sánchez, *Sci. Adv.* **7**, eabd0719 (2021).
- [48] We neglect here possible long-time tails in the viscous medium—a case to which all our results can be generalized.
- [49] M. S. Green, *J. Chem. Phys.* **20**, 1281 (1952).
- [50] H. Mori, *Prog. Theor. Phys.* **33**, 423 (1965).
- [51] R. Kubo, *Reports Prog. Phys.* **29**, 306 (1966).
- [52] N. Van Kampen, *Phys. Rep.* **124**, 69 (1985).
- [53] N. Van Kampen and I. Oppenheim, *Physica A* **138**, 231 (1986).
- [54] U. Seifert, *Rep. Prog. Phys.* **75**, 126001 (2012).
- [55] C. Maes and S. Steffenoni, *Phys. Rev. E* **91**, 022128 (2015).
- [56] M. Krüger and C. Maes, *J. Phys. Condens. Matter* **29**, 064004 (2017).
- [57] G. W. Ford, M. Kac, and P. Mazur, *J. Math. Phys.* **6**, 504 (1965).
- [58] A. Caldeira and A. Leggett, *Phys. A Stat. Mech. its Appl.* **121**, 587 (1983).
- [59] J. Schofield and I. Oppenheim, *Phys. A Stat. Mech. its Appl.* **187**, 210 (1992).
- [60] C. Maes, *Phys. Rev. Lett.* **125**, 208001 (2020).
- [61] J. Reichert and T. Voigtmann, (2020), arXiv:2010.13769 [cond-mat.soft].
- [62] J. Reichert, L. F. Granz, and T. Voigtmann, *Eur. Phys. J. E* **44**, 27 (2021).
- [63] T. V. Kasyap, D. L. Koch, and M. Wu, *Phys. Fluids* **26**, 081901 (2014).
- [64] E. W. Burkholder and J. F. Brady, *Phys. Rev. E* **95**, 052605 (2017).
- [65] P. Pietzonka and U. Seifert, *J. Phys. A: Math. Theor.* **51**, 01LT01 (2018).
- [66] E. W. Burkholder and J. F. Brady, *J. Chem. Phys.* **150**, 184901 (2019).
- [67] Y. Pomeau and P. Résibois, *Phys. Rep.* **19**, 63 (1975).
- [68] S. Hanna, W. Hess, and R. Klein, *J. Phys. A: Math. Gen.* **14**, L493 (1981).
- [69] H. van Beijeren, *Rev. Mod. Phys.* **54**, 195 (1982).
- [70] J. Boon and S. Yip, *Molecular Hydrodynamics* (Dover Publications, New York, 1991).
- [71] O. Bénichou, A. Bodrova, D. Chakraborty, P. Illien, A. Law, C. Mejía-Monasterio, G. Oshanin, and R. Voituriez, *Phys. Rev. Lett.* **111**, 260601 (2013).
- [72] P. Illien, O. Bénichou, C. Mejía-Monasterio, G. Oshanin, and R. Voituriez, *Phys. Rev. Lett.* **111**, 038102 (2013).
- [73] T. R. Kirkpatrick, D. Belitz, and J. V. Sengers, *J. Stat. Phys.* **109**, 373 (2002).
- [74] A. Dhar, *Adv. Phys.* **57**, 457 (2008).
- [75] H. Spohn, in *Lect. Notes Phys.*, Vol. 921 (Springer, Cham, 2016) pp. 107–158.
- [76] L. D’Alessio, Y. Kafri, and A. Polkovnikov, *J. Stat. Mech: Theory Exp.* **2016**, 23105 (2016).
- [77] P. Weinberg, M. Bukov, L. D’Alessio, A. Polkovnikov, S. Vajna, and M. Kolodrubetz, *Phys. Rep.* **688**, 1 (2017).
- [78] S. Hanna, W. Hess, and R. Klein, *Physica A* **111**, 181 (1982).
- [79] O. Granek, Y. Kafri, and J. Tailleur, in preparation.
- [80] See Supplemental Material, which cites Ref. [91], for simulation and computation details.
- [81] M. E. Cates, *Reports Prog. Phys.* **75**, 042601 (2012).
- [82] K. Kitahara, W. Horsthemke, and R. Lefever, *Phys. Lett. A* **70**, 377 (1979).
- [83] A. P. Solon, Y. Fily, A. Baskaran, M. E. Cates, Y. Kafri, M. Kardar, and J. Tailleur, *Nat. Phys.* **11**, 673 (2015).
- [84] L. Angelani and R. D. Leonardo, *New J. Phys.* **12**, 113017 (2010).
- [85] S. A. Mallory, C. Valeriani, and A. Cacciuto, *Phys. Rev. E* **90**, 032309 (2014).
- [86] The diverging behavior of  $\gamma_T$  sets an upper bound on the time-scale for which this approximation holds, as discussed at the end of the Letter.
- [87] M. Enculescu and H. Stark, *Phys. Rev. Lett.* **107**, 058301 (2011).
- [88] See, e.g., J. Cividini, D. Mukamel, and H. A. Posch, *J. Phys. A: Math. Theor.* **51**, 085001 (2018) and references therein.
- [89] P. K. Ghosh, P. Hänggi, F. Marchesoni, and F. Nori, *Phys. Rev. E* **89**, 062115 (2014).
- [90] A preprint that appeared after this Letter’s submission shows numerical results consistent with our negative active friction prediction in a two-dimensional interacting bath: M. Knezevic, L. E. A. Podgurski, and H. Stark, (2021), arXiv:2109.11218 [cond-mat.soft].
- [91] L. Angelani, A. Costanzo, and R. Di Leonardo, *EPL* **96**, 68002 (2011).

# Supplemental Material for: "The Anomalous Transport of Tracers in Active Baths"

Omer Granek,<sup>1</sup> Yariv Kafri,<sup>1</sup> and Julien Tailleur<sup>2</sup>

<sup>1</sup>Department of Physics, Technion-Israel Institute of Technology, Haifa, 3200003, Israel.

<sup>2</sup>Université de Paris, Laboratoire Matière et Systèmes Complexes (MSC), UMR 7057 CNRS, F-75205 Paris, France.

## CONTENTS

I. Simulation details	7
A. Setup	7
B. Active particles	8
C. Tracer	8
D. Relaxation to the steady state	8
E. Parameters	9
F. Results for softly interacting active particles	9
II. Systematic derivation of the long-time limit of the propagator $p(x, \sigma, t x', \sigma', 0)$	9
III. Finite-size effects	12
A. Steady-state solution	13
B. Friction kernel and force-force correlation	14
IV. Perturbative analysis for symmetric tracers	15

## I. SIMULATION DETAILS

### A. Setup

We simulate one-dimensional non-interacting run-and-tumble particles (RTPs) in the presence of a passive tracer. The tracer interacts with the RTPs via the piecewise linear potential  $V(x)$  depicted in Fig. I.1. The potential has a total width  $L_T = \ell + d$ . Its left end has a slope  $f_0/(1 - \xi)$  and a length  $(1 - \xi)d$ . Its right end has a slope  $f_0/(1 + \xi)$  and a length  $(1 + \xi)d$  so that  $\xi$  is a measure of the tracer's asymmetry. We choose  $f_0$  such that  $\mu f_0 < v$  and the particles can pass over the obstacle, hence mimicking the ability of active particles to circulate around a finite tracer in a narrow two-dimensional channel. In all of our simulations, we set  $\rho_L = \mu = v = \alpha = 1$ . All our simulations were ran until a final time  $T = 10^4$ .

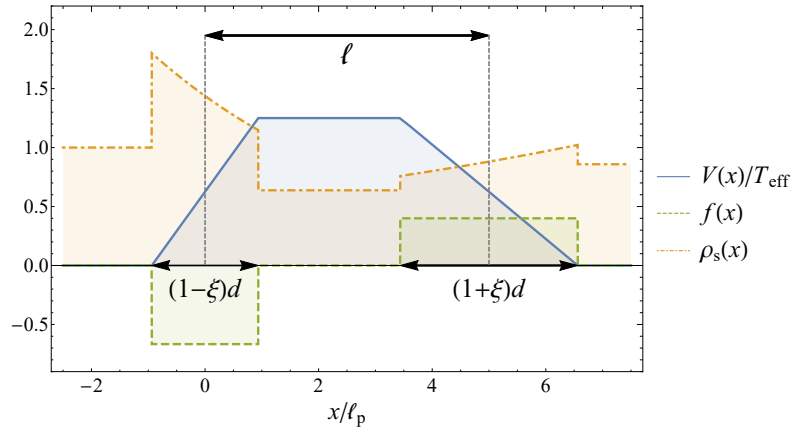


Figure I.1. Tracer potential  $V(x)$  (blue solid line), force  $f(x) = -\partial_x V(x)$  (green dashed line) and steady-state distribution  $\rho_s(x)$  (orange dash-dotted line). In this figure,  $f_0 = d = 1/2$ ,  $\rho_L = \alpha = \mu = v = \ell = 1$ , and  $\xi = 1/4$ .

## B. Active particles

For the time integration of Eq. (7) we employ an Euler time-stepping: the position of a particle  $x_{i+1}$  at time  $t_{i+1} = t_i + \Delta t$  is given by

$$v_i = v\sigma_i + \mu f_i, \quad (\text{I.1})$$

$$x_{i+1} = x_i + v_i \Delta t, \quad (\text{I.2})$$

where  $\sigma_i = \sigma(t_i)$ ,  $f_i = f(x_i - X_i)$ ,  $X_i = X(t_i)$  and  $X_i$  is the left end of the tracer at time  $t_i$ .

The tumbling mechanism is implemented using a continuous-time Monte Carlo method as follows. At time  $t_0 = 0$ , a tumbling time  $\tau_0$  is drawn from an exponential distribution with mean  $2/\alpha$ . For all  $i > 1$ , if  $\tau_0 \notin [t_i, t_{i+1})$ , the integration steps Eqs. (I.1)-(I.2) are performed without change. Otherwise, the integration is done up to  $\tau_0$ , and the next tumbling time  $\tau_1 = \tau_0 + \delta t$  is chosen by sampling  $\delta t$  from an exponential distribution with mean  $2/\alpha$ . The integration of Eqs. (I.1)-(I.2) then continues until  $\min(\tau_1, t_{i+1})$  and the above process is repeated.

A further modification to the time stepping described above is implemented to account for the transitions between the different constant-force regions depicted in Fig. I.1. We denote the boundaries of these regions by  $\{\chi_j\}$  and choose the convention  $\forall x \in [\chi_j, \chi_{j+1})$ ,  $f(\chi_j) \equiv f(x)$ . Then, if, at a given integration step,  $\chi_j \in [x_i, x_{i+1})$ ,  $[t_i, t_{i+1})$  is partitioned into two intervals  $[t_i, t_i + (\chi_j - x_i)/v_i)$  and  $[t_i + (\chi_j - x_i)/v_i, t_{i+1})$  where  $v'_i = v\sigma_i + \mu f_0(\chi_{j+(\sigma_i-1)/2})$ . Then, the particles evolve according to Eqs. (I.1)-(I.2). If a tumbling event occurs within  $[t_i, t_{i+1})$ , the above rule is applied to each of the two intervals before and after the event.

## C. Tracer

For the integration of Eq. (6), we have employed the midpoint algorithm, where the tracer velocity  $U_i = U(t_i)$  and position  $X_i = X(t_i)$  are updated according to

$$U_{i+1} = F_{\text{tot}}^i / \gamma_0, \quad (\text{I.3})$$

$$X_{i+1} = X_i + \frac{U_i + U_{i+1}}{2} \Delta t, \quad (\text{I.4})$$

where  $F_{\text{tot}}^i = F_{\text{tot}}(t_i)$ . For each  $i$ , this integration step is performed after all of the bath particle positions and orientations have been updated according to the previous section. For this reason, and because active particles are integrated using the Eulerian scheme, the midpoint algorithm does not improve beyond the former. However, we have chosen this algorithm as it provides smoother tracer displacement profiles on short time scales. For the towing simulations at constant speed  $U$ , Eq. (I.3) is replaced by  $U_i = U$ .

The piecewise-linear choice of potential and the implementation of the two partitioning mechanisms allow integrating Eq. (7) of the main text *exactly*, given that the tracer is held fixed. Once the tracer moves at a finite velocity, the simulation is subject to a finite accuracy since the tracer position and velocity are updated only after the bath integration step. Since the simulations are performed in the adiabatic limit, this accuracy is very high, as seen from the results presented in the main text.

## D. Relaxation to the steady state

For a given simulation time  $T$ , we set the system size to  $L = vT + L_T$ , so that there are no finite-size corrections to the propagator: an active particle that leaves the tracer at time  $t = 0$  cannot cross the system and return to it from the other side.

We initiate the simulation at time  $t_i = -2T$  with a uniform distribution of orientations and a static tracer at  $X = 0$ . Then, the system is let to relax towards its steady state until time  $t = 0$ , at which the tracer is released and observables are measured up to time  $t = T$ . As shown in Fig. I.2, this protocol is sufficient for the distribution at  $t = 0$  to be undistinguishable from the analytical steady-state. For increased performance, in the towing simulations, the initial distribution was chosen to be the steady-state distribution  $\rho_s(x, \sigma)$  directly. Finally, we verified that all our simulations fall within the adiabatic regime, *i.e.* that  $\langle X(t) \rangle, \langle X^2(t) \rangle_c \ll (D_{\text{eff}} t_i)^{1/2}$  is verified.

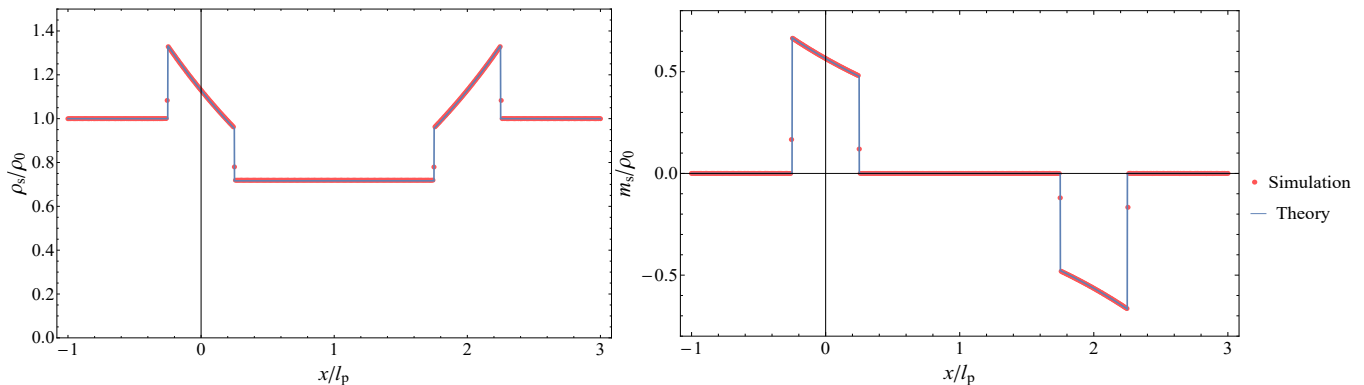


Figure I.2. Steady-state distribution for a symmetric tracer, obtained according to our protocol for a system of size  $L = 4$  and compared to the theoretical prediction. Left: density  $\rho_s(x)$ , right: magnetization  $m_s(x)$ . Here we time-average over  $N = 2 \cdot 10^4$  consecutive snapshots of the system to obtain the histogram. In this figure,  $f_0 = d = 1/2$ ,  $\ell = 2$ ,  $\rho_L = \alpha = \mu = v = 1$ , and  $\xi = 0$ .

### E. Parameters

In the free tracer experiments depicted in Fig. 2a of the main text, we set  $\xi = 0.4$  for the asymmetric tracer. For both tracers we set  $\ell = 1$ ,  $d = 1/2$ ,  $f_0 = 1/2$  and  $\gamma_0 = 10^3$ , which ensures the validity of the adiabatic limit. To obtain the mean-square displacements, we average the square-displacements over  $N = 9800$  realizations of the experiment.

In the towing experiments depicted in Figs. 2b&c, to obtain a higher signal-to-noise ratio, we set  $\ell = 1$ ,  $d = 1/2$ ,  $f_0 = 1/2$  and  $\xi = -0.4749$  for the asymmetric tracer. We average the friction force over  $N = 1200$  realizations, and apply a temporal moving-average filter of width 100. For the symmetric tracer, we set  $\rho_0 = 4$ ,  $f = 1/40$ ,  $d = \ell$  and vary  $\ell$ . We average the friction force over  $N = 10^3 - 10^4$  realizations. To obtain Fig. 2c, we time-average the resulting force over the last two decades  $10^2 \leq t \leq 10^4$ . The relaxation to the asymptotic value of the friction force was verified a posteriori. In all experiments, excluding the towing of a symmetric tracer of size  $L_T = 1$ , the time step was chosen to be  $\Delta t = 10^{-2}$ . For the former, for increased accuracy,  $\Delta t = 2.5 \times 10^{-3}$  was chosen instead.

### F. Results for softly interacting active particles

Here we present numerical results for a bath of pairwise interacting active particles. We consider the interaction potential  $V_{\text{int}}(x) = h(a - |x|)\Theta(a - |x|)$  and set  $a = \ell_p/10$ . We reproduce Fig. 2a of the main text for various values of  $h$  (see Fig. I.3). The asymptotic behaviour on long times agrees well with our theoretical predictions: while the exponents are unaffected by the interactions, the prefactors are renormalized by the interactions. The exponents of the MSDs are universal as expected through the arguments of the main text.

## II. SYSTEMATIC DERIVATION OF THE LONG-TIME LIMIT OF THE PROPAGATOR $p(x, \sigma, t|x', \sigma', 0)$

In the main text, we present a self-contained heuristic derivation of the long-time limit of the propagator given by Eq. (13). For sake of completeness, we present here its systematic derivation. Our method is a perturbation theory for which the small parameter is  $1/t$  as  $t \rightarrow \infty$ .

To proceed, we note that the stochastic differential equation (7) of the main text is equivalent to the master equation for the time-evolution of the probability densities of finding a right-moving and left-moving RTP at position  $x$  and time  $t$ , denoted by  $p_{+1}(x, t)$  and  $p_{-1}(x, t)$ , respectively. The equation reads

$$\partial_t p_\sigma = -\partial_x [(\sigma v + \mu f) p_\sigma] - \frac{\alpha}{2} (p_\sigma - p_{-\sigma}), \quad (\text{II.1})$$

where the force is given by  $f(x) = -\partial_x V(x)$ . The propagator  $p(x, \sigma, t|x', \sigma', 0)$ , for which we use the shorthand notation  $p_\sigma(x, t)$ , is the solution of Eq. (II.1) for the initial condition  $p_\sigma(x, 0) = \delta_{\sigma\sigma'}\delta(x - x')$ . To compute  $p_\sigma(x, t)$ , we note that the

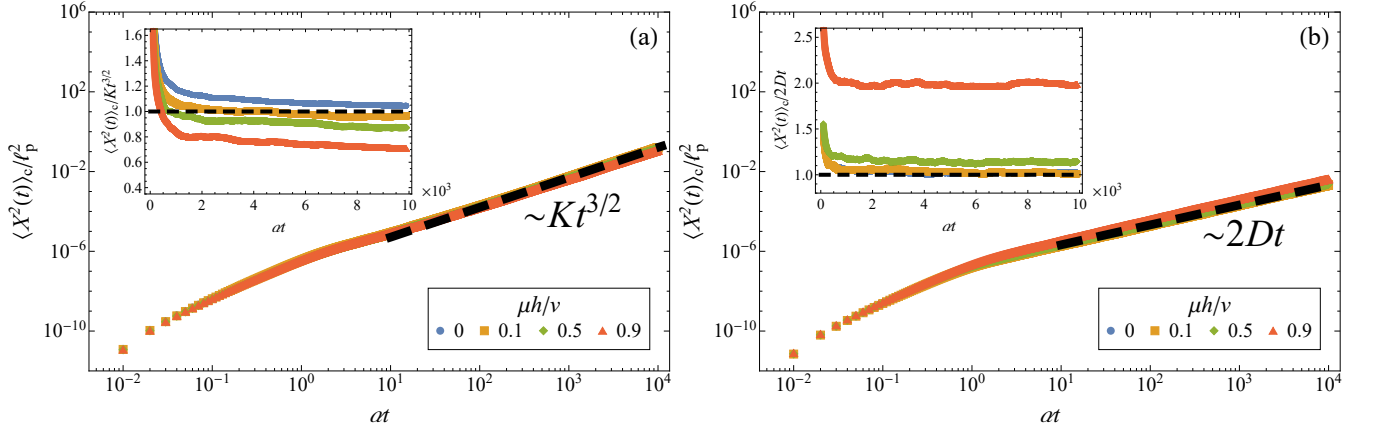


Figure I.3. Simulation results for a tracer in a bath of softly interacting active particles (symbols) compared with our theoretical predictions for the long-time limit of the non-interacting case (dashed black lines). The exponents are unaltered, revealing the universal nature of our predictions. As expected, the prefactor is renormalized by interactions, as illustrated in the insets. (a) Asymmetric tracer and (b) symmetric tracer. Insets: MSDs divided by the theoretical predictions (a moving average filter of width  $100 \alpha^{-1}$  is applied to the data).  $h$  is the amplitude of the interparticle force (see text).

dynamics (II.1), which couple  $\sigma$  and  $-\sigma$ , can be decoupled by applying  $\partial_t$  to both sides of the equation, which leads to

$$0 = (\partial_t^2 + \alpha \partial_t + \partial_x J_\sigma) p_\sigma, \quad (\text{II.2})$$

$$J_\sigma(x, \partial_t) \equiv - \left[ v^2 - (\mu f)^2 \right] \partial_x + \mu [f(\alpha + 2\partial_t) - (\sigma v - \mu f) f']. \quad (\text{II.3})$$

For clarity, we rescale the system as  $t \rightarrow \alpha^{-1}t$ ,  $x \rightarrow \ell_p x$  and  $V \rightarrow T_{\text{eff}}V$ , which is equivalent to setting  $\alpha = \mu = v = 1$ . The result is

$$0 = (\partial_t^2 + \partial_t + \partial_x J_\sigma) p_\sigma, \quad (\text{II.4})$$

$$J_\sigma(x, \partial_t) = - (1 - f^2) \partial_x + [f(1 + 2\partial_t) - (\sigma - f) f']. \quad (\text{II.5})$$

We proceed by taking the Laplace transform of Eq. (II.4) with respect to  $t$ , which yields

$$S_{\sigma\sigma'} \delta(x - x') = [s^2 + s + \partial_x J_\sigma(x, s)] p_\sigma(x, s), \quad (\text{II.6})$$

$$S_{\sigma\sigma'}(x) \equiv [s - \partial_x(\sigma - f(x))] \delta_{\sigma\sigma'} + \frac{1}{2}, \quad (\text{II.7})$$

where  $p_\sigma(x, s) \equiv \int_0^\infty dt e^{-st} p_\sigma(x, t)$  denotes the Laplace transform of  $p_\sigma(x, t)$  and  $\partial_x$  acts on everything to its right. Next, we decompose the current and source operators into force-independent and force-dependent components,

$$J_\sigma = -\partial_x + J_\sigma^f, \quad (\text{II.8})$$

$$S_{\sigma\sigma'} = S_{\sigma\sigma'}^0 + \partial_x f(x) \delta_{\sigma\sigma'}, \quad (\text{II.9})$$

$$J_\sigma^f(x, s) \equiv f^2 \partial_x + [f(1 + 2s) - (\sigma - f) f'], \quad (\text{II.10})$$

$$S_{\sigma\sigma'}^0(x) \equiv (s - \sigma \partial_x) \delta_{\sigma\sigma'} + \frac{1}{2}, \quad (\text{II.11})$$

which allows rewriting Eq. (II.6) as

$$(M_0 + \partial_x J_\sigma^f) p_\sigma = [S_{\sigma\sigma'}^0 + \partial_x f(x) \delta_{\sigma\sigma'}] \delta(x - x'), \quad (\text{II.12})$$

$$M_0 \equiv s^2 + s - \partial_x^2. \quad (\text{II.13})$$

Before solving Eq. (II.12) in the general, it is instructive to consider the case  $f(x) = 0$  to see how the propagator can be

expanded at large times, i.e. for small  $s$ . Since  $f = 0$ , then one also has that  $J_\sigma^f = 0$  and the solution of Eq. (II.12) is

$$p_\sigma^0(x, s) = M_0^{-1} S_{\sigma\sigma'}^0 \delta(x - x') \quad (\text{II.14})$$

$$= \left\{ \frac{1}{2} \left[ \sigma \operatorname{sgn}(x - x') + \frac{s + \frac{1}{2}}{(s^2 + s)^{1/2}} \right] \delta_{\sigma\sigma'} + \frac{1}{4(s^2 + s)^{1/2}} \delta_{\sigma, -\sigma'} \right\} e^{-(s^2 + s)^{1/2} |x - x'|}, \quad (\text{II.15})$$

where  $M_0^{-1} = \int dy G_0(x - y)$  and  $G_0(x - x')$  is the Green's function of  $M_0$ , i.e.

$$M_0(x) G_0(x - x') = \delta(x - x'). \quad (\text{II.16})$$

The solution to this equation is

$$G_0(x - x') = \frac{1}{2(s^2 + s)^{1/2}} e^{-(s^2 + s)^{1/2} |x - x'|} \quad (\text{II.17})$$

$$= \frac{1}{2(s^2 + s)^{1/2}} \sum_{n=0}^{\infty} \frac{(-|x - x'|)^n}{n!} (s^2 + s)^{n/2}. \quad (\text{II.18})$$

Expanding in the limit  $s \ll 1$ , Eq. (II.18) becomes an expansion in powers of  $s^{1/2}$ .

Using the insight gained from the  $f = 0$  case, we look for  $p_\sigma$  in the  $f(x) \neq 0$  case as a series

$$p_\sigma = \frac{1}{s^{1/2}} \sum_{n=0}^{\infty} A_n(x, \sigma | x', \sigma') s^{n/2}, \quad (\text{II.19})$$

where the  $A_n$  need to be determined. In real time, Eq. (II.19) provides the long-time expansion

$$p_\sigma(x, t) = t^{-1/2} \sum_{n=0}^{\infty} \frac{A_{2n}(x, \sigma | x', \sigma')}{\Gamma(\frac{1}{2} - 2n)} t^{-n}. \quad (\text{II.20})$$

Inserting Eq. (II.19) into Eq. (II.6), we arrive at the hierarchy

$$\partial_x [J_\sigma(x, 0) A_0(x, \sigma)] = 0, \quad (\text{II.21})$$

$$\partial_x [J_\sigma(x, 0) A_1(x, \sigma)] = S_{\sigma\sigma'}|_{s=0} \delta(x - x'), \quad (\text{II.22})$$

$$[1 + 2\partial_x f(x)] A_0(x, \sigma) + \partial_x [J_\sigma(x, 0) A_2(x, \sigma)] = 0, \quad (\text{II.23})$$

⋮

This allows us to solve for  $p_\sigma$  perturbatively in the limit  $s \ll 1$ .

Note that both the steady-state  $\rho_s(x, \sigma)$  and  $A_0$  satisfy  $\partial_x (J_\sigma \rho_s) = \partial_x (J_\sigma A_0) = 0$ . It is thus tempting to look for  $A_0$  of the form

$$A_0(x, \sigma | x', \sigma') = N_{\sigma\sigma'}(x') \rho_s(x, \sigma), \quad (\text{II.24})$$

where  $N_{\sigma\sigma'}(x')$  is *a priori* unknown. We now turn to show that this is indeed the case and to determine  $N_{\sigma\sigma'}$ .

First note that the steady-state solution is current free so that, using the notations of Eqs. (II.4) and (II.5),  $J_\sigma(x, 0) \rho_s(x, \sigma) = 0$ . Then, Eq. (II.24) is equivalent to  $J_\sigma(x, 0) A_0(x, \sigma) = 0$  since  $J_\sigma(x, 0)$  is a first-order linear differential operator in  $x$ : by uniqueness of the solution, if both  $A_0$  and  $\rho_s$  are in the kernel of  $J_\sigma$ , then  $A_0(x, \sigma | x', \sigma') = N_{\sigma\sigma'}(x') \rho_s(x, \sigma)$  for some  $N_{\sigma\sigma'}(x')$ .

To show that  $J_\sigma(x, 0) A_0(x, \sigma) = 0$ , we proceed as follows. We use Eq. (II.12) to relate the propagators with the tracer,  $p_\sigma$ , and without the tracer,  $p_\sigma^0$ , and then expand their relationship for small  $s$ . Multiplying both sides of Eq. (II.12) by  $M_0^{-1}$ , we get

$$(1 + M_0^{-1} \partial_x J_\sigma^f) p_\sigma = M_0^{-1} (S_{\sigma\sigma'}^0 + \partial_x f \delta_{\sigma\sigma'}) \delta(x - x') = p_\sigma^0 + M_0^{-1} \partial_x f \delta_{\sigma\sigma'} \delta(x - x'), \quad (\text{II.25})$$

with  $p_\sigma^0$  given in Eq. (II.15) and  $M_0$  defined in Eq. (II.13). Substituting  $M_0^{-1} = \int dy G_0(x-y)$  into Eq. (II.25) then yields

$$p_\sigma^0 = p_\sigma + \int dy G_0(x-y) \partial_y [J_\sigma^f p_\sigma - f \delta_{\sigma\sigma'} \delta(y-x')] \quad (\text{II.26})$$

$$= p_\sigma + \int dy \partial_x G_0(x-y) [J_\sigma^f p_\sigma - f \delta_{\sigma\sigma'} \delta(y-x')] , \quad (\text{II.27})$$

where, in the second equality, we have integrated by parts and used the spatial symmetry of  $G_0$ . Next, we expand for small  $s$ . From Eqs. (II.19) and (II.18) we have that

$$p_\sigma = A_0 s^{-1/2} + \mathcal{O}(s^0) , \quad (\text{II.28})$$

$$p_\sigma^0 = \frac{1}{4} s^{-1/2} + \mathcal{O}(s^0) , \quad (\text{II.29})$$

$$G_0(x-y) = \frac{1}{2} s^{-1/2} + \mathcal{O}(s^0) , \quad (\text{II.30})$$

$$\partial_x G_0(x-y) = -\frac{1}{2} \text{sgn}(x-y) + \frac{1}{2} (x-y) s^{1/2} + \mathcal{O}(s) . \quad (\text{II.31})$$

Substituting these into Eq. (II.27) and equating coefficients at order  $s^{-1/2}$  gives

$$\left[ -\int^x dy J_\sigma(y,0) + \frac{1}{2} \int dy J_\sigma^f(y,0) \right] A_0(y,\sigma) = A_0(x,\sigma) + \left( -\int^x + \frac{1}{2} \int \right) dy J_\sigma^f(y,0) A_0(y,\sigma) \quad (\text{II.32})$$

$$= \frac{1}{4} , \quad (\text{II.33})$$

where, in the first equality, we have used Eq. (II.8). Differentiating Eq. (II.33) with respect to  $x$  then yields  $J_\sigma(x,0) A_0(x,\sigma) = 0$ .

To determine  $N_{\sigma\sigma'}(x')$ , we insert the solution into Eq. (II.32). Using  $J_\sigma(x,0) A_0(x,\sigma) = 0$  and Eqs. (II.8) and (II.24), we get

$$J_\sigma^f(x,0) A_0(x,\sigma|x',\sigma') = \partial_x A_0(x,\sigma|x',\sigma') = N_{\sigma\sigma'}(x') \partial_x \rho_s(x,\sigma) . \quad (\text{II.34})$$

Therefore,

$$\int dy J_\sigma^f(y,0) A_0(y,\sigma|x',\sigma') = N_{\sigma\sigma'}(x') \int dy \partial_y \rho_s(y,\sigma) = \frac{1}{2} N_{\sigma\sigma'}(x') (\rho_R - \rho_L) , \quad (\text{II.35})$$

where we have used  $\rho_s(x,\sigma) = \rho_s(x)/2$  outside the tracer. Finally, Eqs. (II.32)-(II.33) lead to

$$N_{\sigma\sigma'}(x') \left[ \rho_s(x,\sigma) - \int^x dy J_\sigma^f(y,0) \rho_s(y,\sigma) \right] + \frac{1}{4} N_{\sigma\sigma'}(x') (\rho_R - \rho_L) = \frac{1}{4} . \quad (\text{II.36})$$

Choosing any value of  $x$  left of the tracer, for which  $J_\sigma^f(y,0) = 0$  for any  $y \leq x$ , then yields

$$N_{\sigma\sigma'}(x') = \frac{1}{\rho_R + \rho_L} , \quad (\text{II.37})$$

All in all, recalling that  $p_\sigma(x,t) = p(x,\sigma,t|x',\sigma',0)$  and restoring dimensions, we get

$$p(x,\sigma,t|x',\sigma',0) = \frac{\rho_s(x,\sigma)}{\rho_R + \rho_L} (\pi D_{\text{eff}} t)^{-1/2} + \mathcal{O}(t^{-3/2}) , \quad (\text{II.38})$$

which coincides with the heuristic result Eq. (13) of the main text.

### III. FINITE-SIZE EFFECTS

In Section III A, we first review for completeness the steady-state solution of non-interacting RTPs subject to a potential  $V(x)$ , following [82, 83, 91]. This corresponds to Eq. (11) of the main text. We show the solution to apply both to periodic and closed systems, up to finite-size corrections that scale as  $\mathcal{O}(L^{-1})$ .

Then, in Section III B, we bound the finite-size corrections to  $C_{\mathcal{F}}(t)$  and  $\gamma(t)$  and show that Eqs. (14) and (16) of the main

text hold, up to corrections of order  $\mathcal{O}(L^{-1})$ . In the process, we show that the infinite-system-size limit can be obtained equivalently using either closed or periodic systems. This allows us to conduct our simulations using periodic boundary conditions. Throughout our discussion, we make the equations dimensionless by rescaling  $t \rightarrow \alpha^{-1}t$ ,  $x \rightarrow \ell_p x$  and  $V \rightarrow T_{\text{eff}}V$ , which is equivalent to setting  $\alpha = \mu = v = 1$ .

### A. Steady-state solution

Using the notations introduced at the beginning of Section II, the bath density and magnetization are respectively given by  $\rho(x, t) = p_{+1}(x, t) + p_{-1}(x, t)$  and  $m(x, t) = p_{+1}(x, t) - p_{-1}(x, t)$ , up to a common normalization factor that accounts for multiple non-interacting particles. Using Eq. (II.1), one arrives at the dynamics

$$\partial_t \rho = -\partial_x (v m + \mu \rho f), \quad (\text{III.1})$$

$$\partial_t m = -\partial_x (v \rho + \mu m f) - \alpha m. \quad (\text{III.2})$$

In the rescaled variables, the dynamics reduces to

$$\partial_t \rho = -\partial_x (m + \rho f), \quad (\text{III.3})$$

$$\partial_t m = -\partial_x (\rho + m f) - m. \quad (\text{III.4})$$

The equations for the steady-state density  $\rho_s(x)$  and magnetization  $m_s(x)$  are then

$$0 = -\partial_x (m_s + \rho_s f), \quad (\text{III.5})$$

$$0 = -\partial_x (\rho_s + m_s f) - m_s. \quad (\text{III.6})$$

From Eq. (III.5), we obtain the steady-state current

$$J \equiv m_s + \rho_s f = \text{const}. \quad (\text{III.7})$$

Combining Eqs. (III.6) and (III.7) provides the steady-state conditions [91]

$$\{-\partial_x [1 - f^2(x)] + f(x)\} \rho_s(x) = J [1 + \partial_x f(x)], \quad (\text{III.8})$$

$$m_s(x) = J - \rho_s f(x), \quad (\text{III.9})$$

where  $\partial_x$  operates on  $[1 - f^2(x)] \rho_s(x)$ . Using Eq. (III.9), one can express the full steady-state distribution  $\rho_s(x, \sigma)$  using  $\rho_s(x)$  and  $J$  as

$$\rho_s(x, \sigma) = \frac{\rho_s(x) + \sigma m_s(x)}{2} = \frac{1 - \sigma f(x)}{2} \rho_s(x) + \frac{\sigma}{2} J. \quad (\text{III.10})$$

To determine  $\rho_s(x)$  and  $J$ , one now has to solve Eq. (III.8) with the appropriate boundary conditions.

In a closed system with boundaries at  $\pm L/2$ , the current  $J$  vanishes for any  $L$ . In particular,  $J = 0$  for  $L \rightarrow \infty$ . The solution to Eq. (III.8) is then

$$\rho_s(x) = \frac{\rho_L}{1 - f^2(x)} \exp \left[ \int_{-L}^x dy \frac{f(y)}{1 - f^2(y)} \right], \quad (\text{III.11})$$

where  $\rho_L$  is the density left of the tracer. Using Eq. (III.10) and (III.9), one obtains

$$\rho_s(x, \sigma) = \frac{\frac{1}{2} \rho_L}{1 + \sigma f(x)} \exp \left[ \int_{-L}^x dy \frac{f(y)}{1 - f^2(y)} \right]. \quad (\text{III.12})$$

This validates the current-free solution in Eq. (11) for infinite or finite and closed systems.

For periodic systems,  $J \neq 0$ , and the validity of Eq. (11) as a large- $L$  limit of the solution on a ring should be justified. The

general, unnormalized, solution  $\rho_s^{\text{per}}(x)$  to Eq. (III.8) on a ring reads

$$\rho_s^{\text{per}}(x) = \frac{e^{\int_{-L/2}^x dy \frac{f(y)}{1-f^2(y)}}}{1-f^2(x)} \left\{ \rho_L - J \left[ f(x) e^{-\int_{-L/2}^x dy \frac{f(y)}{1-f^2(y)}} + \int_{-L/2}^x dy \frac{e^{-\int_{-L/2}^y dz \frac{f(z)}{1-f^2(z)}}}{1-f^2(y)} \right] \right\}. \quad (\text{III.13})$$

Using the periodic boundary condition  $\rho_s^{\text{per}}(-L/2) = \rho_s^{\text{per}}(L/2)$  yields

$$J = \rho_L \frac{e^{\int_{-L/2}^{L/2} dx \frac{f(x)}{1-f^2(x)}} - 1}{\int_{-L/2}^{L/2} dx \frac{e^{\int_x^{L/2} dy \frac{f(y)}{1-f^2(y)}}}{1-f^2(x)}} = \rho_L \frac{e^{\int_{-L/2}^{L/2} dx \frac{f(x)}{1-f^2(x)}} - 1}{\frac{L-L_T}{2} \left[ e^{\int_{-L/2}^{L/2} dx \frac{f(x)}{1-f^2(x)}} + 1 \right] + L_T I_0}, \quad (\text{III.14})$$

where we use the definitions of the main text and introduce

$$I_0 \equiv \int_0^{L_T} dx \frac{e^{\int_y^{x_R} dy \frac{f(y)}{1-f^2(y)}}}{L_T (1-f^2(x))}. \quad (\text{III.15})$$

For  $L \gg 1$ , we obtain the familiar result

$$J = -\frac{F}{L} \left[ 1 + \mathcal{O}\left(\frac{L_T}{L}\right) \right], \quad (\text{III.16})$$

where  $F = -(\rho_R - \rho_L)$ . Expectedly, Eq. (III.16) shows that the current vanishes as  $L \rightarrow \infty$ . In this limit, we obtain

$$\rho_s^{\text{per}}(x) = \left( 1 + \frac{F}{2\rho_0} \right) \rho_s(x), \quad (\text{III.17})$$

where  $\rho_0 = (\rho_R + \rho_L)/2$ . Therefore, the infinite-size limit of solutions in closed and periodic systems differs only by an overall multiplicative constant. Rescaling the density as

$$\rho_0 \rightarrow \frac{\rho_0}{1 + \frac{F}{2\rho_0}}, \quad (\text{III.18})$$

leads to the same density profile as in the closed case and thus validates Eq. (11) for the periodic case as well. Note that, under this rescaling,  $\rho_L \rightarrow \rho_0$ .

## B. Friction kernel and force-force correlation

To conclude the section, we show that the finite-size corrections to Eqs. (14) and (16) are  $\mathcal{O}(L^{-1})$ . We first note that we can use the expression (13) for the propagator, which is derived in an infinite system, as long as the time is such that  $t \ll L^2$  so that the boundaries of the system are not reached by RTPs that interact with the obstacle at  $t = 0$ .

We now want to show that the measurement of the force-force correlations in periodic systems, given by

$$C_{\mathcal{F}}^{\text{per}}(t) = \sum_{\sigma\sigma'} \int dx dx' f(x) p(x, \sigma, t | x', \sigma', 0) f(x') \rho_s^{\text{per}}(x', \sigma'), \quad (\text{III.19})$$

indeed yields, to leading order in  $L^{-1}$ ,  $C_{\mathcal{F}}(t)$  as predicted by Eq. (14). We first note that, since  $f(x)$  has compact support,  $C_{\mathcal{F}}^{\text{per}}(t)$  remains finite as  $L \rightarrow \infty$  irrespective of the boundary conditions. Then, up to the rescaling given in Eq. (III.18),  $\rho_s(x', \sigma')$  and  $\rho_s^{\text{per}}(x', \sigma')$  coincide up to corrections of order  $\mathcal{O}(L^{-1})$ . The force-force correlations predicted by Eq. (14) in the main text thus coincide with those measured in periodic systems, up to the rescaling (III.18) and corrections of order  $\mathcal{O}(L^{-1})$ .

We now turn to show that the same holds for the friction

$$\gamma^{\text{per}}(t) = \sum_{\sigma\sigma'} \int dx dx' f(x) p(x, \sigma, t | x', \sigma', 0) \partial_{x'} \rho_s^{\text{per}}(x', \sigma'). \quad (\text{III.20})$$

In contrast to  $C_{\mathcal{F}}^{\text{per}}$ , the finiteness of  $\gamma^{\text{per}}(t)$  should be verified for large periodic systems because of the integral over  $x'$  in

Eq. (III.20). Dividing the integration domain into the region inside the tracer  $\mathcal{T} = \{0 < x < L_T\}$  and outside of the tracer  $\mathcal{T}^c$ , we obtain

$$\begin{aligned} \gamma^{\text{per}}(t) &= \sum_{\sigma\sigma'} \int dx \left( \int_{\mathcal{T}} dx' + \int_{\mathcal{T}^c} dx' \right) f(x) p(x, \sigma, t | x', \sigma', 0) \partial_{x'} \rho_s^{\text{per}}(x', \sigma') \\ &= \sum_{\sigma\sigma'} \int dx \int_{\mathcal{T}} dx' f(x) p(x, \sigma, t | x', \sigma', 0) \partial_{x'} \rho_s^{\text{per}}(x', \sigma') - \frac{J}{2} \sum_{\sigma\sigma'} \int dx \int_{\mathcal{T}^c} dx' f(x) p(x, \sigma, t | x', \sigma', 0), \end{aligned} \quad (\text{III.21})$$

where, in the second equality, we used Eqs. (III.8) and (III.10), which give  $\partial_{x'} \rho_s^{\text{per}}(x', \sigma') = \partial_{x'} \rho_s^{\text{per}}(x')/2 = -J/2$  outside the tracer. Since  $J \sim -F/L$  (see Eq. (III.16)), one finds that

$$-\frac{J}{2} \sum_{\sigma\sigma'} \int dx \int_{\mathcal{T}^c} dx' f(x) p(x, \sigma, t | x', \sigma', 0) = \frac{1}{2} F \int dx f(x) p_U(x, t) + \mathcal{O}\left(\frac{L_T}{L}\right), \quad (\text{III.22})$$

where the probability density  $p_U(x, t) \equiv \int dx' p(x, t | x', 0) \cdot L^{-1}$  is the propagation of an initially uniform distribution  $p_U(x, 0) = L^{-1}$ . Because  $|f(x)| < 1$ , every point in the system is accessible by the dynamics. This implies that  $p_U(x, t)$  is spread over the entire system with a non-negligible density at each point. In conjunction with normalization of probability,  $\int dx p_U(x, t) = 1$ , it implies that  $p_U(x, t) \sim L^{-1}$ . Since  $f(x) = 0$  outside of the tracer, it follows that  $F \int dx f(x) p_U(x, t)/2 = \mathcal{O}(L_T/L)$ . We conclude that  $\gamma^{\text{per}}(t)$  remains finite as  $L \rightarrow \infty$ , and can be obtained from  $\gamma(t)$  by rescaling the density according to Eq. (III.18). As claimed, the leading order correction to Eq. (16) is  $\mathcal{O}(L^{-1})$ .

#### IV. PERTURBATIVE ANALYSIS FOR SYMMETRIC TRACERS

Here we derive the scaling forms for the force-force correlation of a symmetric tracer given by Eq. (22) of the main text, together with the scaling function  $G$ , as well as for the friction coefficients given by Eqs. (23-26) of the main text. To do so, we use a systematic perturbative analysis for a piecewise linear tracer (see Fig. IV.1). We start with a perturbation theory in  $d/\ell_p$  and then consider the small  $f_0$  (and  $d$ ) limit. Once more, we make the equations dimensionless by rescaling  $t \rightarrow \alpha^{-1}t$ ,  $x \rightarrow \ell_p x$  and  $V \rightarrow T_{\text{eff}}V$ .

We begin with the  $d \ll \ell_p$  limit and now turn to derive Eq. (22) and its accompanying (correct) scaling function

$$G(y) = \frac{1 - \left(\frac{2\mu f_0 y}{v}\right)^2}{\left[1 - \left(\frac{\mu f_0}{v}\right)^2\right]^2}, \quad (\text{IV.1})$$

which, upon rescaling the equations, becomes

$$G(y) = \frac{1 - (2f_0 y)^2}{(1 - f_0^2)^2}. \quad (\text{IV.2})$$

For any point  $x$  outside the tracer sides, the leading-order contribution in  $d$  to the propagator is given by the free propagator Eq. (II.15). However, inside the tracer sides, there is a correction due to the jump of the propagator at the side edges (see Fig. IV.1). To obtain this correction, we integrate Eq. (II.1) over a small region  $[x - \varepsilon, x + \varepsilon]$ , for any value of  $x$ , and take  $\varepsilon \rightarrow 0$ . This results in

$$[1 + \sigma f(x)] p(x, \sigma, s | x', \sigma')|_{-}^{+} = \sigma \delta_{\sigma\sigma'} 1_{xx'}, \quad (\text{IV.3})$$

where  $g|_{-}^{+} \equiv g(x^+) - g(x^-)$  and  $1_{xx'} = 1$  if  $x = x'$  and is 0 otherwise. (Note that we have reinstated the explicit dependence on the initial values  $x'$  and  $\sigma'$  in  $p$ .) This means that  $p(x, \sigma, s | x', \sigma')$  changes with  $x$  in two ways: It jumps discontinuously at the boundaries of the side regions—where  $f$  is discontinuous—and at  $x = x'$ , according to Eq. (IV.3). It varies continuously elsewhere. Furthermore, in the  $d \ll 1$  limit, the continuous change within each of the narrow tracer sides  $\mathcal{R} = [-d/2, d/2]$  and  $\mathcal{L} = [L_T - d/2, L_T + d/2]$  can be neglected to leading order. This means that  $p(x, \sigma, s | x', \sigma')$  is piece-wise constant within  $\mathcal{R}$  and  $\mathcal{L}$ , with the plateau values being determined by the jumps at  $x = x'$  and on the edges of those regions, using Eq. (IV.3) and that the solution outside the tracer sides is  $p^0(x, \sigma, s | x', \sigma')$ . In sum, the leading-order expansion is

$$p(x, \sigma, s | x', \sigma') = \frac{p_{\sigma}^0(x, \sigma, s | x', \sigma')}{1 + \sigma f(x)} + \mathcal{O}(d). \quad (\text{IV.4})$$

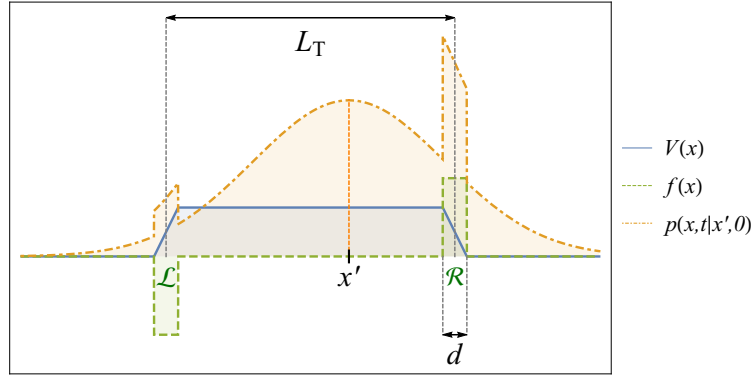


Figure IV.1. Schematic description of the influence of the tracer (blue potential; solid line) for  $d \ll 1$ . Outside the forcing regions  $\mathcal{R}$  and  $\mathcal{L}$  (green dashed line), the leading-order contribution to the propagator  $p(x, t|x', 0) = \sum_{\sigma\sigma'} p(x, \sigma, t|x', \sigma', 0)$  (orange dash-dotted line) for long times  $t \gg 1$  is given by the solution in free space. Inside the regions, the dominant modification is a constant multiplicative shift.

Likewise, expanding Eq. (11) gives

$$\rho_s(x', \sigma') = \frac{\rho_0}{2[1 + \sigma' f(x')]} + \mathcal{O}(d). \quad (\text{IV.5})$$

Eqs. (IV.4) and (IV.5) are then used to compute  $C_{\mathcal{F}}(s) \equiv \mathcal{L}[C_{\mathcal{F}}(t)](s)$  and  $\gamma(s) = \mathcal{L}[\gamma(t)](s)$ , where  $\mathcal{L}[g(t)](s) \equiv \int_0^\infty dt e^{-st} g(t)$  is the Laplace transform. By definition, we get

$$C_{\mathcal{F}}(s) = \sum_{\sigma\sigma'} \int dx dx' f(x) p(x, \sigma, s|x', \sigma') f(x') \rho_s(x', \sigma'), \quad (\text{IV.6})$$

$$\gamma(s) = \sum_{\sigma\sigma'} \int dx dx' f(x) p(x, \sigma, s|x', \sigma') \partial_{x'} \rho_s(x', \sigma'). \quad (\text{IV.7})$$

Using the tracer symmetry, Eq. (IV.6) becomes

$$C_{\mathcal{F}}(s) = 2 \frac{\rho_0 (f_0 d)^2}{1 - f_0^2} \sum_{\sigma\sigma'} \frac{1 + \sigma' f_0}{2} p(x, \sigma, s|0, \sigma')|_{L_T}^0 + \mathcal{O}(d^3), \quad (\text{IV.8})$$

Using Eqs. (II.15), (IV.4) and (IV.5) and expanding for  $s \ll 1$  then gives

$$C_{\mathcal{F}}(s) = \frac{\rho_0 (f_0 d)^2}{(1 - f_0^2)^2} \left[ L_T - \frac{1}{2} (L_T^2 - 4f_0^2) s^{1/2} \right] + \mathcal{O}(d^3, s^{3/2}). \quad (\text{IV.9})$$

In real time, the coefficients of  $s^{1/2}$  in the  $s \ll 1$  expansions become the coefficients of  $-(4\pi)^{-1/2} t^{-3/2}$  in the  $t \gg 1$  expansions, yielding

$$C_{\mathcal{F}}(t) = \frac{\rho_0 (f_0 d L_T)^2}{4\pi^{1/2} t^{3/2}} G(L_T^{-1}) + \mathcal{O}(d^3, t^{-5/2}), \quad (\text{IV.10})$$

where  $G(y)$  is given by Eq. (IV.2). Upon restoring the dimensions, Eq. (IV.10) becomes Eq. (22), with  $G(y)$  given by Eq. (IV.1) as claimed. Additionally, Eq. (IV.9) provides the noise intensity

$$I = \int_0^\infty dt C_{\mathcal{F}}(t) = C_{\mathcal{F}}(s=0) = \frac{\rho_0 (f_0 d)^2}{(1 - f_0^2)^2} L_T + \mathcal{O}(d^3), \quad (\text{IV.11})$$

which remains positive irrespective of  $L_T$ .

We proceed to obtain the scaling forms for  $\gamma_p(t)$ ,  $\gamma_a(t)$  and  $\gamma_T$  given in the main text. The change in the sign of  $\gamma(s)$  can be observed by analysing the  $f_0 \ll 1$  and  $d \ll 1$  limit. For this, we use the decomposition  $\gamma(s) = \gamma_p(s) - \gamma_a(s)$  where  $\gamma_p = \mathcal{L}[\gamma_p(t)](s)$  and  $\gamma_a = \mathcal{L}[\gamma_a(t)](s)$ . We also note that  $p_\sigma = p_\sigma^0 + \mathcal{O}(f_0)$  and  $\rho_s(x', \sigma') = \rho_0/2 + \mathcal{O}(f_0)$ . Using Eqs. (23)

and (24) in combination with Eq. (II.15) then gives

$$\gamma_p = \frac{C_{\mathcal{F}}(s)}{1 - f_0^2} = \rho_0(f_0 d)^2 \left( L_T - \frac{d}{3} \right) - \frac{1}{2} \rho_0(f_0 d L_T)^2 s^{1/2} + \mathcal{O}(f_0^3, s^{3/2}), \quad (\text{IV.12})$$

$$\gamma_a = 2\rho_0 f_0^2 d + \mathcal{O}(f_0^3, s^{3/2}), \quad (\text{IV.13})$$

which leads to  $\gamma_a(t) \sim \mathcal{O}(f_0^3)t^{-3/2}$  of the main text. Moreover, Eqs. (IV.12)-(IV.13) yield

$$\gamma_T = \int_0^\infty dt \gamma(t) = \gamma_p(s=0) - \gamma_a(s=0) = \rho_0(f_0 d)^2 \left( L_T - \frac{d^2 + 6}{3d} \right) + \mathcal{O}(f_0^3), \quad (\text{IV.14})$$

which, upon restoring dimensions, provides Eq. (26). As seen in Eq. (IV.14),  $\gamma_T$  becomes negative for  $L_T \lesssim (d^2 + 6)/3d$ . Note that, since each term in Eq. (IV.14) is proportional to at least one power of  $d$ , the expansion is valid for  $d \ll 1$ . In fact, its range of validity can be extended up to  $d = \mathcal{O}(1)$ .